J Porous Mater (2018) 25:129–136
DOI 10.1007/s10934-017-0426-x

Mesoporous aluminosilicate: efficient and reusable catalysts for esterification of *sec*-butanol with acetic acid

Ankana Phukan[1] · Siddhartha Kumar Bhorodwaj[1] · Podma Pollov Sharma[1] · Dipak Kumar Dutta[1]

Published online: 19 April 2017

Abstract Esterification of acetic acid with *sec*-butanol to produce *sec*-butyl acetate has been systematically carried out by using mesoporous (3–9 nm size) aluminosilicate (meso-AS) catalysts (surface area 327–578 $m^2\ g^{-1}$) derived from Na-montmorillonite by controlled HCl acid activation. High catalytic activity up to 89% conversion with nearly 100% selectivity towards *sec*-butyl acetate is observed. The effect of reaction temperature, mole ratio of reactants and catalyst concentration on esterification reactions were studied. The catalyst could be recycled and reused several times without significant loss of their catalytic activities. The catalysts were characterized by pyridine adsorbed FT-IR, XRD, SEM-EDX, MAS-NMR, surface area (BET) and TPD analysis.

Keywords Mesoporous-aluminosilicate · Montmorillonite K-10 · Esterification · Heterogeneous catalyst · *Sec*-butyl acetate

1 Introduction

Esterification of carboxylic acids with alcohols to produce esters has been recognized as one of the most important reactions due to the wide utility of esters as plasticizers, solvents, flavour chemicals, precursors for pharmaceuticals, agrochemicals and other fine chemicals [1, 2]. The esterification of a secondary alcohol is much more difficult to achieve compared to primary alcohols. The steric effect of the substrates and the lower nucleophilicity of the oxygen atom hinder the formation of the corresponding ester [3]. Conversions are also limited by slow reaction rates and reversible reactions. Conventional homogenous catalysts widely used in industries for esterification include H_2SO_4, HCl, HF, H_3PO_4, and $ClSO_2OH$ [4, 5]. However, these liquid acid catalysts suffer from several drawbacks, such as their corrosive nature, the existence of side reactions and the fact that the catalysts cannot be easily separated from the reaction mixture [6]. Due to stringent and growing environmental regulations, the chemical industry needs the development of more eco-compatible synthetic methodologies [7]. The use of heterogeneous acid catalysts offers an alternative development and has received a considerable attention in the recent past [6]. The heterogeneous catalysts reported in the literature for esterification reactions include ion exchange resin [8], H-ZSM–5 [9], zeolites-Y [10], niobic acid [11], sulphated oxides [12] and supported dodecatungstophosphoric acid, $H_3PW_{12}O_{40}$ on acid modified montmorillonite clay [13]. In fact, there is a need to develop esterification of *sec*-butanol with acetic acid using more environmental friendly solid acid catalyst. In recent years, the use of solid acid catalysts, such as acid treated montmorillonite clay, has received considerable attention in different areas of organic synthesis, because of their environmental compatibility, reusability, operational simplicity, non-toxicity, non-corrosiveness, low cost and easy isolation [14]. Montmorillonite is di-octahedral clay of smectite group and is composed of stacked alumino-silicate layers. It possesses some unique properties such as cation exchange capacity, intercalation, swelling etc. which allow

Electronic supplementary material The online version of this article (doi:10.1007/s10934-017-0426-x) contains supplementary material, which is available to authorized users.

✉ Dipak Kumar Dutta
dipakkrdutta@yahoo.com

[1] Materials Sciences and Technology Division, Advanced Materials Group, North-East Institute of Science and Technology (CSIR), Jorhat, Assam 785 006, India

modifications to its structural as well as textural properties for efficient catalysis. The commonly used modification methods are acid activation, cation exchange, intercalation and pillaring [15]. Acid activated montmorillonite clay is one of the widely studied solid acid catalysts for many organic transformations such as isomerisation [16], alkylation [17, 18], acylation [19] and other reactions [20]. Acid activated clay minerals also have great potential as inexpensive and efficient supports [21] owing to their chemical and mechanical stability, high surface area and structural properties [22]. The treatment of purified montmorillonite clay with mineral acid has been reported to replace exchangeable cations with H^+ ions and leaching Al^{3+} out of both tetrahedral and octahedral sites but leaving the SiO_4 group largely intact. Such acid treated clays are therefore partially delaminated and exhibit higher surface area, pore volume, pore diameter [23] and higher surface acidity [24] which results into their improved adsorption and catalytic properties. Here, we report an environmental friendly mesoporous aluminosilicate catalyst developed by controlled HCl acid leaching of montmorillonite clay and their high catalytic activity of Bronsted acid catalysed esterification of *sec*-butanol with acetic acid.

2 Experimental

2.1 Materials and methods

Natural montmorillonite clay (procured from Gujarat Mines Bentonite, India) contains silica sand, iron oxide, etc. as impurities and was purified by standard sedimentation method [25] to collect the <2 µm fraction (rich in montmorillonite). The oxide composition of the clay determined by weight chemical and flame photometric methods were: SiO_2: 49.42; Al_2O_3: 20.02; Fe_2O_3: 7.49; MgO: 2.82; CaO: 0.69; LOI: 17.51; others (Na_2O, K_2O and TiO_2) 2.05%. The clay was converted in to homoionic Na-exchanged form (Na-Mont.) by stirring in 2 M NaCl solution for about 72 h, which was washed and finally dialyzed against distilled water until conductivity of the dialyzate approached to that of distilled water [26, 27].

2.2 Preparation of mesoporous aluminosilicate catalysts

Three gram of dry Na-Mont. powder was treated with 100 ml of 4 M HCl. The slurry was refluxed for different time intervals (15 min, 1, 2 and 4 h). After cooling, the slurry was filtered with suction, washed with distilled water and finally dialyzed against distilled water till the conductivity of the dialyzate approached to that of distilled water and showed negative test for Cl^- with silver nitrate [28]. The mass was then dried at 50 ± 5 °C in air oven to obtain the solid product. The samples are designated as meso-AS-15 min, meso-AS-1 h, meso-AS-2 h and meso-AS-4 h corresponding to their periods of acid activation.

2.3 Catalyst characterization

FTIR studies of purified and acid activated montmorillonites were carried out by using Perkin-Elmer system 2000 FTIR spectrometer. Specific surface area, pore volume, average pore diameter were measured by using Autosorb1 (Quantachrome, USA). Surface areas were determined by N_2 gas adsorption at 77 K and applying Brunner-Emmett-Teller (BET) method. Prior to adsorption, samples were degassed at 200 °C for about 1.5 h. Pore size distributions were derived from desorption isotherms using the Barrett-Joyner-Halenda (BJH). Thin layered (oriented) samples were prepared on glass slides by standard technique for basal spacing (d_{001}) determination by XRD. Diffraction patterns were taken in the range $2\Theta = 2–60°$ at a rate of 6° min^{-1} (X-ray diffractometer JEOL, JDX-11p 3 A, Japan). ^{29}Si and ^{27}Al MAS NMR spectra of selected samples were recorded in a DSX 300 NMR spectrometer. Scanning electron microscopy (SEM) images and energy dispersive X-ray spectroscopy (EDX) patterns were obtained from the samples by using Carl Zeiss SIGMA FE-SEM operated at 5 and 20 KV and Oxford X-Max 20 EDS detector. Prior to examination, samples were lightly coated with gold. Cation exchange capacities of different samples were determined by using standard techniques [29]. Acidity of meso-AS catalysts were determined by NH_3-TPD measurement using Chem BET Pulsar (Quantachrome, USA). The samples were prepared by outgassing at 140 °C under He gas flow. NH_3 gas was passed through the samples for 30 min for complete saturation and then free absorbed NH_3 was removed by passing He for another 30 min. NH_3-TPD analysis was achieved by heating the samples at 20 °C min^{-1} under He gas flow rate at 80 ml min^{-1}. The analyses were carried out in the temperature range 100–800 °C. The types of acidity measurement of meso-AS catalysts were also carried out by pyridine-adsorbed FT-IR analysis. The samples were first finely ground and allowed to adsorb pyridine in a closed chamber for 30 min and followed by removal of excess absorbed pyridine on the samples by keeping in a hot air oven at 120 °C for 1 h. Samples were analyzed in a FT-IR spectrophotometer.

2.4 Esterification reaction

0.3 g of freshly activated catalyst (dried at 120 °C for 2 h in an oven), 0.15 mol of acetic acid (Merck, 99.8%), 0.05 mol of *sec*-butanol (Merck, 98%) were taken into a pressure autoclave. The autoclave temperature was then slowly

raised to 100, 125, 150 and 200 °C (autogeneous pressure) and maintained at the desired temperature during the specified reaction periods (2, 6 and 9 h). The reaction products were collected from the autoclave and analyzed by GC (Chemito GC, Model 8510, FID). The catalyst was washed with water and activated for next experiments.

3 Results and discussion

The most important requirement for porous solid acid catalysts for use in liquid-phase processes is pore size which should be large enough to allow rapid diffusion of reactants in to the pores and the products need to come out. In general, there is a wide interest in the use of mesoporous aluminosilicate catalysts like acid modified clays in different catalytic reactions [30–35] as they possess tailorable pore sizes in the mesoporous range (typically 2–50 nm). The mesopores in such catalysts allow the reactants to access additional active sites in the pores and results in improved rates of acid catalysis [36]. The suitability of mesoporous aluminosilicate catalysts obtained by acid modification of clay, particularly smectite, to promote Bronsted or Lewis acid-catalysed reactions depend on the extent of leaching of the raw clay which, in turn, depends upon the acid treatment conditions [37]. The solid acid catalysts which are reusable and readily separable from reaction products are of much interest for replacement of hazardous and corrosive liquid acids.

The mesoporous aluminosilicate catalysts were synthesized from Na-montmorillonite by controlled HCl acid activation for different time intervals. The N_2 adsorption–desorption study confirmed the mesoporous nature of such catalysts. The adsorption–desorption isotherms of different catalysts (Fig. 1a) show the form of Type IV isotherms with the hysteresis loop of type H3, which is a characteristic of a mesoporous solid. The pore size distribution plot in Fig. 1b shows that the average pore sizes of such catalysts are in the range of 2–10 nm suggesting that pore sizes of the catalysts lie in the mesoporous region. The surface area of Na-montmorillonite as determined by using Brunner-Emmett-Teller (BET) method was found to be 101 $m^2\ g^{-1}$

Acid activation of Na-montmorillonite for 15 min (meso-AS-15 min) and 1 h (meso-AS-1 h) caused an increase in the surface area to 395 and 578 $m^2\ g^{-1}$ respectively and the pore diameter to 3.06 and 4.12 nm respectively (Table 1) because of considerable leaching of Al from the clay structure.

Further acid activation up to 2 h (meso-AS-2 h) and 4 h (meso-AS-4 h) caused a decrease in surface area to 400 and 327 $m^2\ g^{-1}$ respectively, which is due to open up the existing pores by destroying the internal walls of the pores without significantly changing the overall pore volume. The oxide compositions of different meso-AS as determined by weight chemical and flame photometric methods (Supporting Information, Table S1) confirmed the leaching of Al from the clay structure as the percentage of Al_2O_3 goes on decreasing as the time of acid activation increases. Total acidity of different meso-AS catalysts were determined by TPD analysis (Table 1). A typical NH_3-TPD profile of meso-AS-15 min is presented below (Fig. 2) showing maximum acidic sites in the strong acidic region (400–600 °C) [38, 39].

The extraction of octahedral or tetrahedral Al^{3+} ions from the clay during acid activation was investigated by ^{27}Al and ^{29}Si MAS-NMR spectroscopy. The ^{27}Al

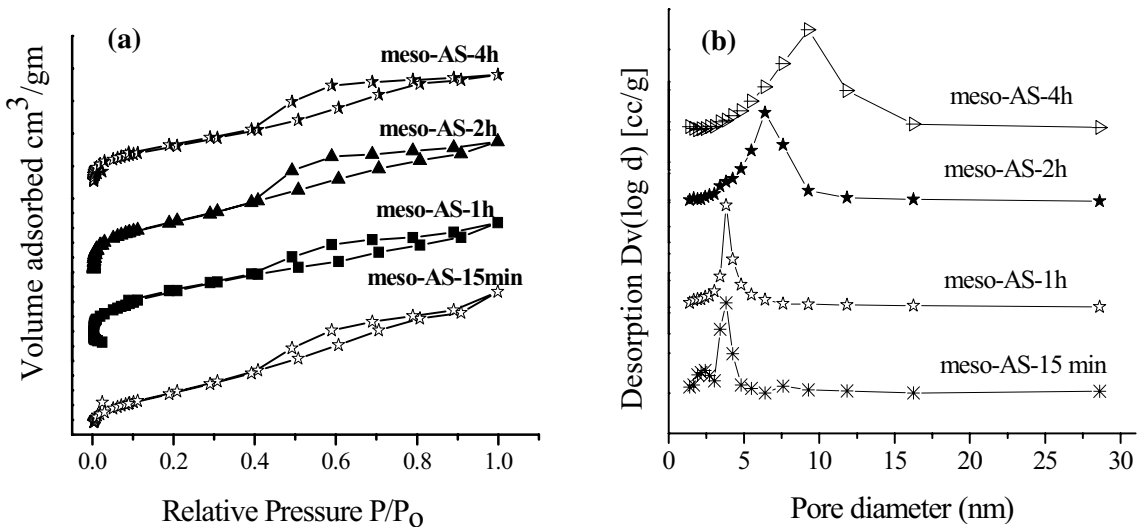

Fig. 1 **a** N_2 adsorption–desorption isotherms of different catalysts. **b** Pore size distribution curves of different catalysts determined by applying BJH method

Table 1 Surface area, cation exchange capacities (CEC), pore volume, average pore diameter and conversion on esterification of acetic acid with *sec*-butanol

Sample	Surface area ($m^2\ g^{-1}$)	CEC (meq/100 g)	Acidity (mmol g^{-1})	Pore diameter (nm)	Pore volume (cc g^{-1})	Conversion* (%)
meso-AS-15 min	395	96	0.41	3.06	0.302	89
meso-AS-1 h	578	41	0.43	4.12	0.596	81
meso-AS-2 h	400	20	0.56	6.03	0.603	77
meso-AS-4 h	327	7	0.59	8.48	0.761	64
Montmorillonite K10**	230	35	0.20	6.63	0.441	5.5

*Reaction conditions: temperature: 150 °C (closed system), pressure: autogeneous, reaction time: 9 h, catalyst amount: 0.3 g, acid: alcohol: 3:1 (mole ratio).**Ref. [40]

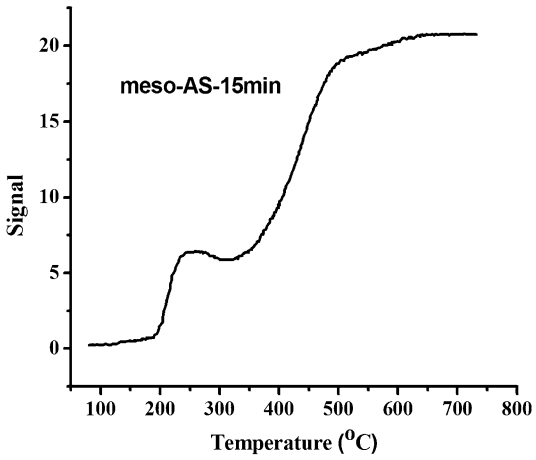

Fig. 2 NH_3-TPD profile for meso-AS-15 min

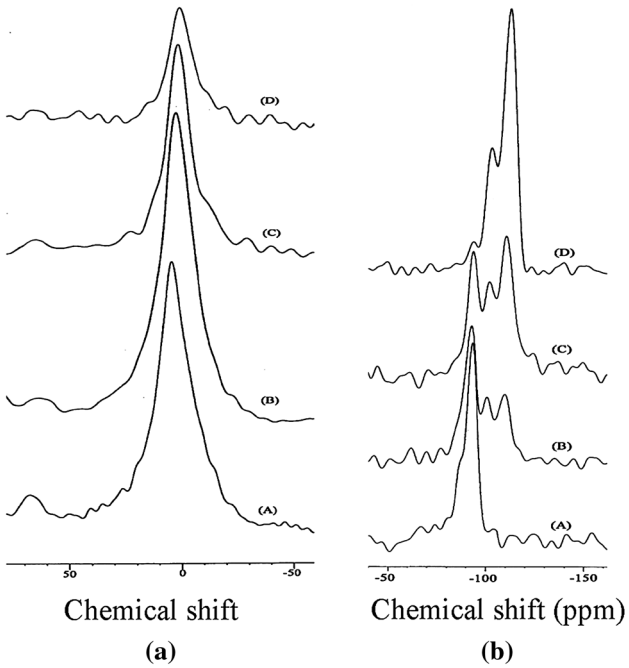

Fig. 3 **a** ^{27}Al and **b** ^{29}Si MAS NMR spectra of *a* Na-montmorillonite, *b* meso-AS-15 min, *c* meso-AS-2 h and *d* meso-AS-4 h

MAS-NMR (Fig. 3a) spectra of untreated montmorillonite showed octahedrally (intense signal at δ = 3.92 ppm) and tetrahedrally (weak signal at δ = 67 ppm) coordinated alumina in the framework of the clay. The ^{27}Al MAS-NMR spectra indicated that during acid activation, the intensity of the peak due to octahedral Al decreased along with shifting the peak position from 3.92 to about 1.6 ppm for acid treatment period of upto about 4 h, but the peak value at δ = 67 ppm due to tetrahedral Al remained almost similar to untreated montmorillonite indicating residual intact of the tetrahedral Al structure. It was observed that during the initial acid treatment period upto 15 min, the peak intensity of meso-AS-15 min did not differ much with that of Na-montmorllonite. However, distinct differences of peak intensities were noticed at the long acid treatment periods of 2–4 h due to adequate leaching of Al^{3+} from octahedral sites. Generally, the high surface area of such mesoporous aluminosilicate catalysts is related to the removal of octahedral Al from the clay structure. A maximum surface area can be obtained when some or all the tetrahedral aluminium remain in the structure. The ^{29}Si MAS-NMR spectra of Na-montmorillonite and other mesoporous aluminosilicate catalysts are presented in Fig. 3b. .

Untreated montmorillonite contained one sharp peak at δ = −93 ppm $Q^3(0Al)$ due to SiO_4 tetrahedra surrounded by three other silicate units in the tetrahedral sheet and one Al (or Mg) atoms through oxygen bridges of montmorillonite. With the increase in the acid treatment time, the intensity of this peak, i.e. δ = −93 ppm $Q^3(0Al)$ of montmorillonite, gradually disappeared with simultaneous appearance of the new peaks at about δ = −111 ppm [$Q^4(0Al)$ (Si–O–Si bond)] and δ = −102 ppm [(SiO_3) Si–OH bond]. After prolong acid treatment, the intensity of the signal at δ = −111 ppm [$Q^4(0Al)$ (Si–O–Si bond)] increased, showing the decomposition of a large amount of montmorillonite. The SEM image (Fig. 4a) revealed that the surface of such mesoporous catalyst was rough and the EDX analysis (Fig. 4b) showed a predominant amount of Si on the surface of the clay after acid

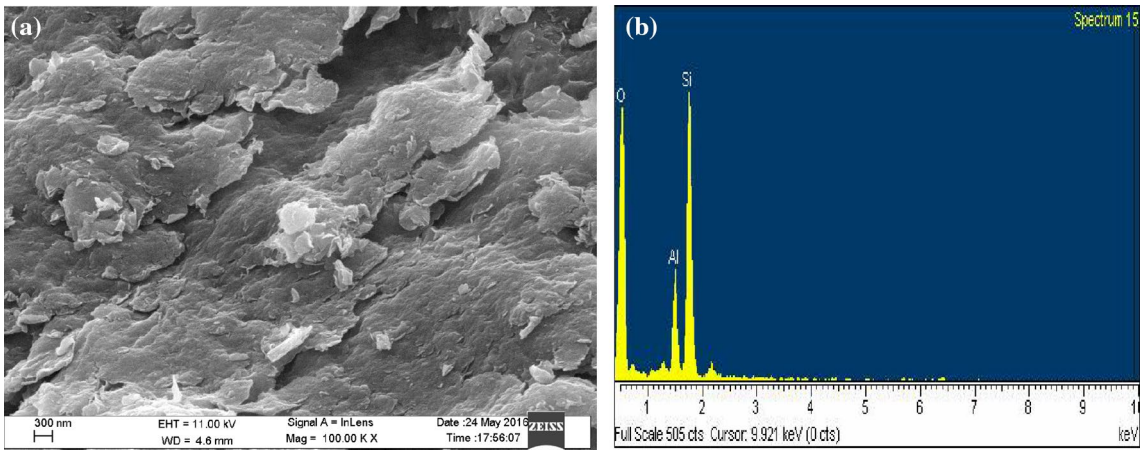

Fig. 4 **a** SEM image and **b** EDX spot analysis of meso-AS-1 h

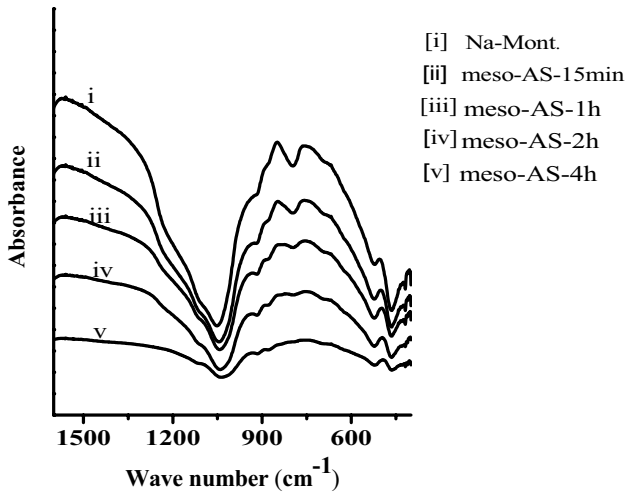

Fig. 5 FTIR spectra of purified and acid activated montmorillonite clays

activation, indicating leaching of the Al from the surface matrix.

The FTIR spectra of purified Na-montmorillonite (Na-Mont.) and meso-AS reflect the structural degradation of the clay components and formation of an amorphous silica phase during acid activation (Fig. 5). The complex absorption band of the Si–O stretching vibrations of Na-Mont. lies approximately at 1040 cm^{-1}. The shape and position of this band changed during acid activation. The band shifts from 1040 to 1095 cm^{-1}, indicating the change in bonding environment in tetrahedral layer and formation of an amorphous silica phase.

The cation exchange capacities (CEC) of the different meso-AS catalysts decreased (Table 1) as the time of acid activation was increased which was due to the gradual destruction of the layered structure of the clay. This observation was also substantiated by the progressive loss of intensity and broadening of the d_{001} reflection in X-ray diffraction patterns of different samples (Supporting Information, Fig S1). An approximately linear relationship was observed for different meso-AS catalysts when CEC was plotted as a function of percentage of Al_2O_3 present on meso-AS catalysts and it (Supporting Information, Fig S2) reveals that with the increase in acid activation time, the number of exchangeable cation sites removed was in proportion to the extent of extraction of octahedral Al^{3+} ions. It is interesting to observe (Table 1) that the catalyst meso-AS-1h, exhibiting the highest surface area 578 $m^2\ g^{-1}$ shows a lower conversion 81% than that of the catalyst, meso-AS-15 min, with surface area 395 $m^2\ g^{-1}$, exhibiting the highest conversion 89%. In case of the catalyst montmorillonite K10, with the lowest surface area 230 $m^2\ g^{-1}$ shows the lowest conversion i.e. 5.5% only. Therefore it indicates that surface area of the catalysts is not only the factor responsible for conversion. Acid activation up to 15 min as in case of meso-AS-15 min did not delaminate much of the layer structure of the clay and therefore the leached octahedral Al^{3+} ions from the lattice may occupy the place of interlamellar cation exchange sites and polarized the coordinated water molecule and form Al_2OH and releases H^+ [40, 41] which in turn, increases the Bronsted acidity and leads to the highest conversion i.e. 89%. But acid activation for 1 h destroys the layer structure of the clay to a greater extent and therefore Al^{3+} ions were removed from the interlayer regions, which decreased the Bronsted acidity of meso-AS-1 h. Further acid activation for 2 and 4 h caused more destruction of the layer structures and leading to decreased conversions 77 and 64% respectively. However, for montmorillonite K10, the lowest conversion (5.5%) was observed even with considerable CEC value of 35 meq/100 g. It is observed that, (Table 1) with the increase in acid treatment time, total acidity increases but conversion decreases. This increase in acidity

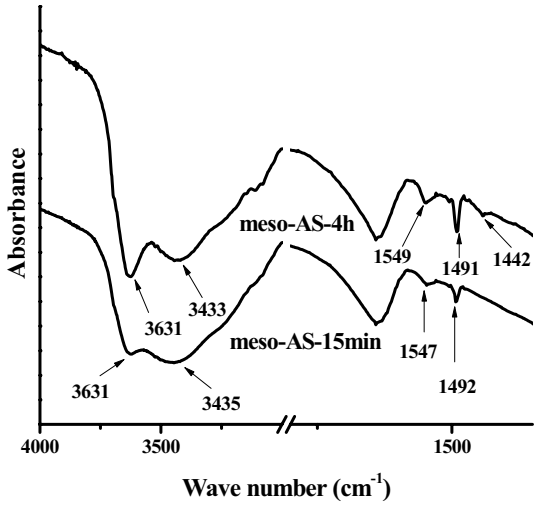

Fig. 6 Pyridine adsorbed FT-IR spectra of meso-AS-15 min and meso-AS-4 h

was due to the increased generation of Lewis acidity on the acid activated clay. Pyridine adsorbed FTIR study of meso-AS-15 min and meso-AS-4 h (Fig. 6) show characteristic IR absorption for Bronsted acid sites at 1547 and 1549 cm^{-1} respectively, which is due to the C–C stretching vibration of pyridinium ion attached to the Bronsted acid sites indicating the generation of Bronsted acidity on both 15 min and 4 h activation time. In addition, meso-AS-4 h shows a band at 1442 cm^{-1} which is a characteristic peak of C–C stretching vibration of coordinatively bonded pyridine complex to the Lewis acid sites indicating the generation of Lewis acidity which is absent in meso-AS-15 min. This indicates that the Lewis acidity increases on enhancing acid activation time. The bands at 1491 and 1492 cm^{-1} present on meso-AS-4 h and meso-AS-15 min are due to C–C stretching of pyridine bonded to total acid sites [42, 43]. The band (Fig. 6) observed near 3631 cm^{-1} is due to silanol (Si–OH) groups exposed at the external layer surface generated by both 15 min and 4 h activation, while broad bands near 3433 and 3435 cm^{-1} are due to Al_2OH groups formed in the interlayer region. The relative intensity of bands for interlayer Al_2OH decreases while for silanol groups (Si–OH) increases with time of activation. This may be correlated to the leaching of Al^{3+} ions during acid activation with increase in time [40].

Thus the results substanciate that esterification of *sec*-butanol with acetic acid is primarily catalysed by Bronsted acidity instead of Lewis acidity which even on increasing by enhancing acid activation time leading to total higher acidity shows lower conversion. Thus, meso-AS-15 min, having highest cation exchange capacity (96 meq/100 g), higher Bronsted acidity, lower surface area (395 $m^2\ g^{-1}$), lower pore diameter (3.06 nm) and lower pore volume (0.302 cc g^{-1}), appeared to be the most efficient catalyst for the liquid phase esterification of *sec*-butanol with acetic acid.

A detail study on the influence of reaction time on the acetic acid conversion using meso-AS-15 min as catalyst was carried out. A gradual increase in the conversion was seen (Fig. 7) with the increase in reaction period. It revealed that at 9 h of reaction time, about 89% conversion was obtained which does not enhance even the reaction time was increased. The sudden increase in the conversion of the esterification reaction during the period above 6 h upto 9 h might be due to maintenance of favorable equilibrium condition of the reaction leading to higher production rate which might be caused because of involvement of critical concentration factors of the several components present in the reaction vessel.

The reaction was carried out at various reaction temperatures, ranging from 100 to 200 °C at a given acetic acid to *sec*-butanol ratio of 3:1 for 1 and 9 h using meso-AS-15 min as catalyst. Upon raising the reaction temperature, the conversion of acetic acid was found to be increased (Supporting Information, Fig S3) because it favors the formation of carbonium ion from acetic acid, which in turn reacts with *sec*-butyl alcohol to produce *sec*-butyl acetate (Scheme 1). The plausible mechanism involved in the esterification of acetic acid with *sec*-butanol is shown in the Scheme 1. The esterification reaction of acetic acid with *sec*-butanol is an electrofilic substitution reaction which follows Eley–Rideal mechanism where protons chemisorbed on the catalyst surface attacked the acid molecule first and form a stable carbocation. The carbocation is then attacked by one of the

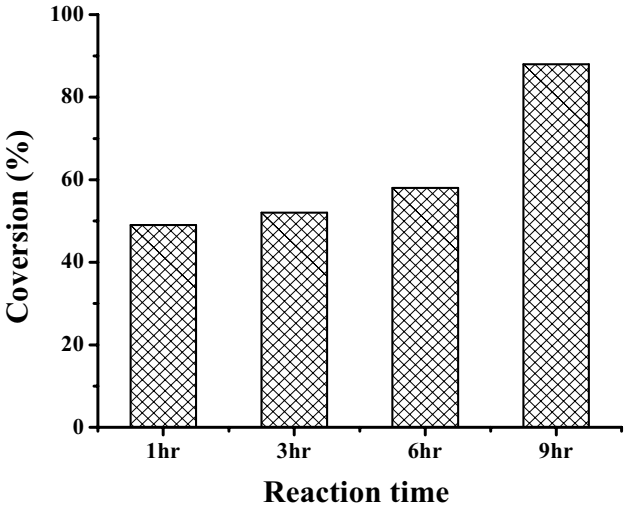

Fig. 7 The effect of reaction time on the esterification of acetic acid with *sec*-butanol using meso-AS-15 min, Reaction conditions: temperature: 150 °C (closed system), pressure: autogeneous, catalyst amount: 0.3 g, acid: alcohol: 3:1 (mole ratio)

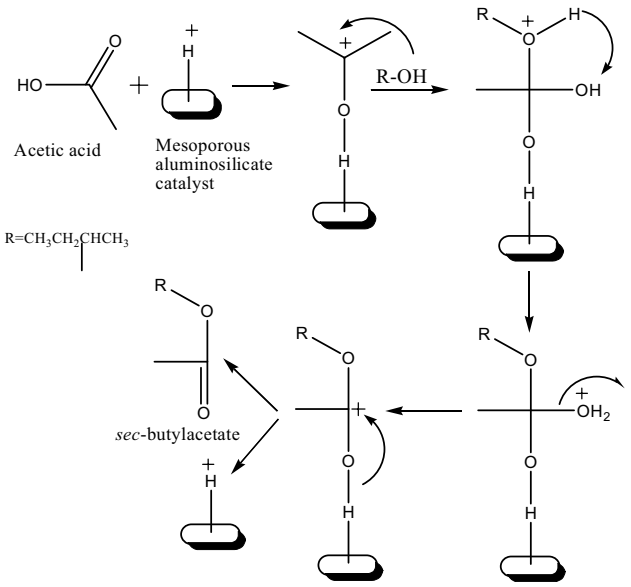

Scheme 1 Mechanism of esterification of acetic acid with *sec*-butanol

lone pair of *sec*-butanol and results a unstable intermediate which finally releases one water molecule and gives the product *sec*-butyl acetate along with the regeneration of the catalyst.

While investigating the effects of catalyst amounts, it was observed that the conversion of *sec*-butyl alcohol increased marginally with the increase in catalyst amounts (Fig. 8). This was due to diffusional resistance in catalyst pores as the reactions on porous catalyst involve adsorption and diffusion of reactants through the pores. The product molecules remained adsorbed within the pores/channels of the catalyst and might restrict diffusion for the fresh reactants.

The effects of the mole ratios of the reactants on the esterification for 1 and 9 h were tested (Fig. 9). The conversion was found to be maximum with 3:1 mol ratio of acetic acid to *sec*-butanol and *sec*-butyl acetate was observed as the only product, i.e. selectivity is 100%.

The catalyst was found to be reusable with no significant loss in activity even after three cycles. A marginal decrease in conversion was observed i.e. the conversion of 89% in the first run decreases to about 85 and 83% in the 2nd and 3rd run respectively. Though the catalyst was separated and washed after each reaction to remove all the adsorbed reactants and products, retention of some of the adsorbed reactants and products species are still possible, which might cause the blockage of active sites and cause a decrease in catalytic activity.

4 Conclusion

The mesoporous aluminosilicates (meso-AS) catalysts were prepared from Na-montmorillonite by controlled HCl acid activation for different time intervals (15 min, 1, 2 and 4 h) exhibiting high surface area in the range 327–578 $m^2\ g^{-1}$, surface acidity 0.41–0.59 mmol g^{-1}, and pore diameter 3.06–8.48 nm. The esterification of acetic acid with *sec*-butanol catalysed by meso-AS-15 min catalyst showed high conversion 89% with nearly 100% selectivity towards *sec*-butyl acetate. The meso-AS catalysts offer several advantages such as good yields of products, leaching free

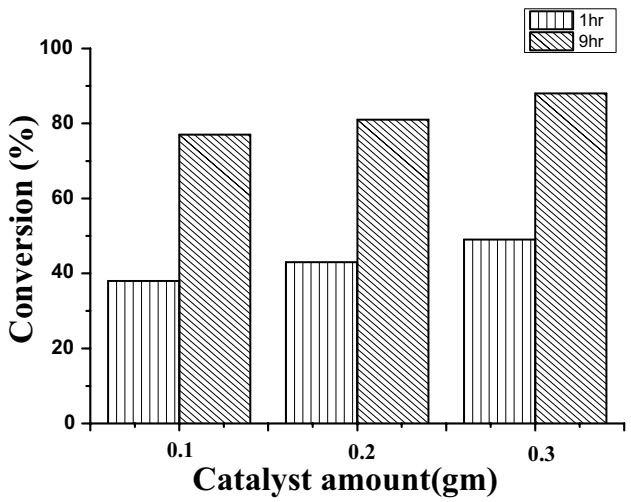

Fig. 8 The effect of catalyst amount on the esterification of acetic acid with *sec*-butanol using meso-AS-15 min. Reaction conditions: temperature: 150 °C (closed system), pressure: autogeneous, reaction time: 1 and 9 h, acid:alcohol: 3:1 (mole ratio)

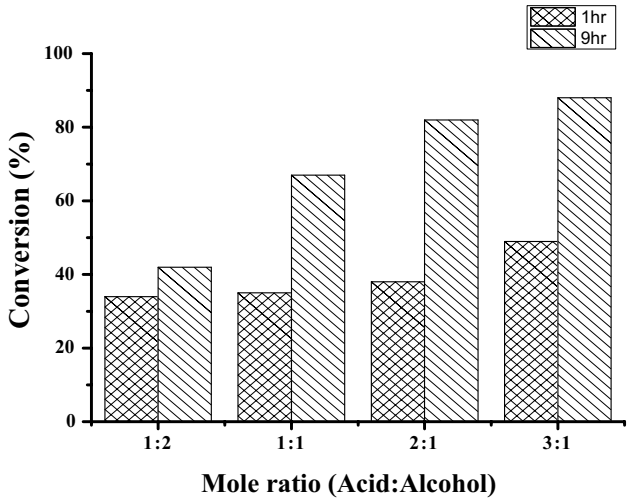

Fig. 9 The effect of mole ratio on the esterification of acetic acid with *sec*-butanol Reaction conditions: temperature: 150 °C (closed system), pressure: autogeneous, reaction time: 1 and 9 h, catalyst amount: 0.3 g

catalytic operation, inexpensive and environmental friendly catalytic system. The catalysts are also found to remain active for several runs without significant loss of activity.

Acknowledgements The authors are grateful to Dr. D. Ramaiah, Director, CSIR-North-East Institute of Science and Technology, Jorhat, Assam, India, for his kind permission to publish the work. The authors thank Dr. P. Sengupta, Head, Materials Sciences and Technology Division, CSIR-NEIST, Jorhat, for his encouragement. Thanks are also given to CSIR, New Delhi for a financial support (Network projects: CSC-0125, 0135 and MLP-6000/1).

References

1. W.B. Pan, F.R. Chang, L.M. Wei, M.J. Wua, Y.C. Wua, Tetrahedron. Lett. **44**, 331–334 (2003)
2. A. Zaidi, J.L. Gainer, G. Carta, Biotechnol. Bioeng. **48**, 601–605 (1995)
3. I.L. Shih, L.C. Chiu, C.T. Lai, W.C. Liaw, D.F. Tai, Biotechnol. Lett. **19**, 857–859 (1997)
4. M.N. Timofeeva, M.M. Matrosova, T.V. Reshetenko, L.B. Avdeeva, A.A. Budneva, A.B. Ayupov, E.A. Paukshtis, A.L. Chuvilin, A.V. Volodin, V.A. Likholobov, J. Mol. Catal. A **211**, 131–137 (2004)
5. D.P. Sawant, A. Vinu, J. Justus, P. Srinivasu, S.B. Halligudi, J. Mol. Catal. A **276**, 150–157 (2007)
6. T.A. Peters, N.E. Benes, A. Holmen, J.T.F. Keurentjes, Appl. Catal. A **297**, 182–188 (2006)
7. R. Ballini, G. Bosica, R. Maggi, M. Ricciutelli, P. Righi, G. Sartori, R. Sartorio, Green Chem. **3**, 178–180, (2001).
8. J. Gimenez, J. Costa, S. Cervera, Ind. Eng. Chem. **26**, 198–202 (1987)
9. Z.H. Bin, Z. Kui, Y.Z. Young, Z. Wei, L.H. Xuan, J. Nat. Gas Chem. **6**, 228–236 (1997)
10. A. Corma, H. Garcia, S. Iborra, J. Primo, J. Catal. **120**, 78–87 (1989)
11. Z.H. Chen, T. Lizuka, K. Tanabe, Chem. Lett. **13**, 1085–1088 (1984)
12. M. Hino, K. Arata, Chem. Lett. **12**, 1671–1672 (1981)
13. S.K. Bhorodwaj, D.K. Dutta, Appl. Catal. A **378**, 221–226 (2010)
14. G. Song, B. Wang, H. Luo, L. Yang, Catal. Commun. **8**, 673–676 (2007)
15. N.N. Binitha, S. Sugunan, Catal. Commun. **8**, 1793–1797 (2007)
16. M.K. Yadav, C.D. Chudasama, R.V. Jasra, J. Mol. Catal. A **216**, 51–59 (2004)
17. C.N. Rhodes, M. Franks, G.M.B. Parkes, D.R. Brown, Chem. Commun. **12**, 804–807 (1991)
18. M.P. Hart, D.R. Brown, J. Mol. Catal. A **212**, 315–321 (2004)
19. R.V. Jasra, Bull. Catal. Soc. India **2**, 157–183 (2003)
20. D. Bhuyan, L. Saikia, D.K. Dutta, Appl. Catal. A **487**, 195–201 (2014)
21. O.S. Ahmed, D.K. Dutta, Langmuir **19**(13), 5540–5541 (2003)
22. W. Wang, H. Chen, A. Wang, Sep. Purif. Technol. **55**, 157–164 (2007)
23. O.S. Ahmed, D.K. Dutta, J. Mol. Catal. A **229**, 227–231 (2005)
24. B. Tyagi, C.D. Chudasama, R.V. Jasra, Spectrochim. Acta, Part A **64**, 273–278 (2006)
25. J.E. Gillott, *Clay in Engineering, Geology*, 1st edn. (Elsevier, Amsterdam, 1968) (Chap. 11)
26. A. Phukan, J.N. Ganguli, D.K. Dutta, J. Mol. Catal. A **202**, 279–287 (2003)
27. M. Bora, J.N. Ganguli, D.K. Dutta, Thermochim. Acta **346**, 169–175 (2000)
28. O.S. Ahmed, D.K. Dutta, Thermochim. Acta **395**, 209–216 (2003)
29. A.B. Searle, R.W. Grimshaw, *The Chemistry and Physics of Clays and Other Ceramic Materials*, 3rd ed. (Earnest Benn, London, 1960) (Chap. 5)
30. H.H.P. Yiu, D.R. Brown, Catal. Lett. **56**, 57–64 (1998)
31. F.R.B.D. Marcos, Catal. Rev. Sci. Eng. **37**, 1–100 (1995)
32. S.R. Chitnis, M.M. Sharma, React. Funct. Polym. **32**, 93–115 (1997)
33. A. Vaccari, Catal. Today **41**, 53–71 (1998)
34. R.S. Varma, Tetrahedron **58**, 1235–1255 (2002)
35. Z. Ding, J.T. Kloprogge, R.L. Frost, G.Q. Lu, H.Y. Zhu, J. Porous Mater. **8**, 273–293 (2001)
36. T. Caio, T. Atsushi, I. Ai, T. Kajuhiro, N.K. Junko, E. Kohki, H. Shigenobu, T. Tatsumi, D. Kazunari, Angew. Chem. Int. Ed. **49**, 1128–1132 (2010)
37. P. Komadel, M. Janek, J. Madejova, A. Weekes, C. Breen, Faraday Trans. **93**, 4207–4210 (1997)
38. A. Azzouz, D. Nistor, D. Miron, A.V. Ursu, T. Sajin, F. Monette, P. Niquette, R. Hausler, Thermochim. Acta **449**, 27–34 (2006)
39. F. Lonyi, J. Valyon, Microporous Mesoporous Mater. **47**, 293–301 (2001)
40. U. Flessner, D.J. Jones, J. Roziere, J. Zajac, L. Storaro, M. Lenarda, M. Pavan, A. Jimenez-Lopez, E. Rodriguez-Castellon, M. Trombetta, G. Busca, J. Mol. Catal. A **168**, 247–256 (2001)
41. C.R. Reddy, G. Nagendrappa, B.S. Jai Prakash, Catal. Commun. **8**, 241–246 (2007)
42. J. Wang, J. Ren, X. Liu, J. Xi, Q. Xia, Y. Zu, G. Lu, Y. Wang, Green Chem. **14**, 2506–2512 (2012)
43. S. Ramesh, B.S.J. Prakash, Y.S. Bhat, Appl. Clay Sci. **48**, 159–163 (2010)